

Light Induced Charge Transfer from Transition-metal Doped Aluminium Clusters to Carbon Dioxide

Alexandra Göbel,[†] Angel Rubio,^{†,‡,¶} and Johannes Lischner^{*,§}

[†]*Max Planck Institute for the Structure and Dynamics of Matter, Center for Free Electron
Laser Science, Hamburg, Germany.*

[‡]*Nano-Bio Spectroscopy Group and European Spectroscopy Facility (ETSF), Universidad
del País Vasco CFM CSIC-UPV/EHU-MPC & DIPC, 20018 Donostia-San Sebastián,
Spain.*

[¶]*Center for COmputational Quantum Physics, Simons Foundation Flatiron Institute, New
York, NY, USA.*

[§]*Department of Materials, Imperial College London, London SW7 2AZ, UK. The Thomas
Young Centre for Theory and Simulation of Materials, London SW7 2AZ, UK.*

E-mail: alexandra.goebel@mpsd.mpg.de, angel.rubio@mpsd.mpg.de, j.lischner@imperial.ac.uk

Abstract

Charge transfer between molecules and catalysts plays a critical role in determining the efficiency and yield of photo-chemical catalytic processes. In this paper, we study light-induced electron transfer between transition metal doped aluminium clusters and CO₂ molecules using first-principles time-dependent density-functional theory. Specifically, we carry out calculations for a range of dopants (Zr, Mn, Fe, Ru, Co, Ni and Cu) and find that the resulting systems fall into two categories: Cu- and Fe-doped clusters exhibit no ground state charge transfer, weak CO₂ adsorption and light-induced

electron transfer into the CO₂. In all other systems, we observe ground state electron transfer into the CO₂ resulting in strong adsorption and predominantly light-induced electron back-transfer from the CO₂ into the cluster. These findings pave the way towards a rational design of atomically precise aluminium photo-catalysts.

Introduction

Transformation of CO₂ into useful chemicals is currently one of the most important environmental and societal global challenges and there is significant interest in discovering novel catalysts which facilitate such reactions in an environmentally friendly setup.¹⁻⁴ A key intermediate step in this process is the transfer of an electron into the lowest unoccupied molecular orbital (LUMO) of the CO₂ which results in chemical activation.⁵ This can be achieved either thermally,⁶ for example when the molecule is adsorbed at an electron-donating metal site, electro-chemically,⁷ via plasma⁸ or photo-chemically,¹ i.e. through illumination by light.

Homogeneous catalysts, such as [Rh(cod)Cl₂]-Ph₂P(CH₂)₄PPh₂⁹ or "FCAT"¹⁰ have been used to transform CO₂ into useful products, such as formic acid or carbon monoxide. Despite their impressive turn-over frequencies (TOFs),¹¹ homogeneous catalysts are usually expensive to synthesize¹² and separation of the catalyst from the reaction products can be difficult. In addition, homogeneous catalysts can suffer from degradation which can lead to very short life-times.¹⁰ In contrast, heterogeneous catalysts are typically cheaper and easier to fabricate, but exhibit lower yields and are less selective.^{12,13} Common heterogeneous catalytic systems used in CO₂ conversion are Fe based catalysts like Fe-Cu-Al-K(2) which exhibits CO₂ conversion efficiencies of up to 30 %, ¹³ Cu/ZnO catalysts¹⁴ with 15% CO yield and supported Ni catalysts with CO₂ conversion yields of almost 50 %.¹⁵

Atomically defined catalysts have the potential to overcome the challenges described above. Such catalysts consist of well-defined nanostructures composed of a specific number of atoms. They are highly controllable and allow for a detailed understanding of the relationship between structure and activity.¹⁶ For example, [Cu₃₂H₂₀(S₂P(OiPr)₂)₁₂] has been

shown to reduce CO_2 to CO .¹⁷ A lot of research has been focused on atomically defined gold structures.^{16,18,19} Despite the need for further stabilization, e.g. through ligands or immobilization onto surfaces, the atomically defined $\text{Au}_n(\text{SR})_m$ systems have been shown to be robust towards thermal degradation at temperatures up to 200 °C.¹⁶ For example, $[\text{Au}_{25}(\text{SR})_{18}]^-$ was shown to be catalytically active for the electroreduction of CO_2 .²⁰ In addition, the structural effect of doping of this cluster was studied by Fei et. al. in atomically defined $\text{Au}_{24}\text{M}(\text{SR})_{18}$ ($\text{M} = \text{Pt}, \text{Pd}, \text{Hg}, \text{and Cd}$) in which they could show that Hg and Cd are always located in an icosahedron shell position and never at the cluster core.²¹

Aluminium nanostructures have received significant attention in recent years for applications in photocatalysis because of their attractive and highly tunable optical properties.^{22–24} In addition, aluminium is relatively cheap, has one of the highest natural abundances and is easy to process.^{25,26} Due to aluminium’s non-precious character it is very prone to oxidation.²² The formed oxide layer, though, has been shown to be porous and allows for diffusion of small molecules.²⁷ For example, Halas and coworkers performed reverse-water-gas-shift reactions on Al@CuO nanocrystals.²⁸ Halas and coworkers also showed that aluminium nano-crystals can be decorated with different transition-metals (Fe, Co, Ni, Ru, Rh, Pd, Ir and Pt) to increase light absorption and generate hot-spots, making these systems highly interesting for various applications like plasmonic photo-catalysis or surface enhanced spectroscopies.²⁹

To gain a mechanistic understanding of catalytic processes and the effect of dopants, the theoretical modelling of the atomic and electronic structure of (photo-)catalysts is useful. For the case of Al nanostructures, Zhao et al. used first-principles density-functional theory (DFT) to understand the effect of introducing dopant atoms and additional charge on the adsorption of CO_2 .³⁰ They focused on small icosahedral clusters containing 12 Al atoms and one dopant (located at the center of the icosahedron) and found that these systems can activate CO_2 .³¹ However, they only studied ground-state properties of these systems and did not investigate electronic excitations of relevance to photocatalysis.

In this paper, we study charge transfer between transition metal doped aluminium clusters and a CO_2 molecule in both the ground state and the excited state. In particular, we carry out first-principles DFT calculations to determine the relaxed atomic geometry of $[\text{Al}_{12}\text{M}]-\text{CO}_2$ systems (with M denoting Zr, Mn, Fe, Ru, Co, Ni or Cu) and analyze the ground state charge transfer between cluster and CO_2 . Except for the Fe and Cu doped systems, we observe significant electron transfer into the CO_2 which results in chemical activation. Next, we carry out time-dependent density-functional theory (TDDFT) calculations to study the light-induced charge transfer in these systems. For the Fe and Cu doped cluster, we observe light-induced electron transfer into the CO_2 . In contrast, systems with significant ground state charge transfer predominantly exhibit a back-transfer of electrons to the cluster in the excited states. Interestingly, the Zr and Co doped clusters have light-induced charge transfer in both directions.

Methods

We study the atomic and electronic properties of small transition-metal atom doped aluminium clusters with adsorbed CO_2 molecules. In particular, we start from icosahedral $[\text{Al}_{13}]$ and replace one of the outer Al atoms by one of the following atoms: Fe, Mn, Co, Cu, Ni, Ru or Zr. The resulting system is denoted by $[\text{Al}_{12}\text{M}]$ with M being the transition metal.

Next, we place a CO_2 molecule in the vicinity of the transition metal atom and relax the atomic positions using density-functional theory (DFT). We have found that the relaxed structures depend sensitively on the details of the computational approach, including choice of basis, exchange-correlation functional and spin-polarization. To identify low-energy configurations, we first create a pool of candidate structures in the following way: we start by placing a linear CO_2 molecule at a distance of 2.7 Å from the dopant atom with its axis perpendicular to the direction from the dopant to the cluster center. For this starting

configuration, we first carry out a relaxation with spin-unpolarized DFT using the PBE exchange-correlation functional³² with a Grimme D2 correction³³ to capture van-der-Waals interactions. The resulting structures were then used as starting points for a relaxation with spin-polarized DFT. These calculations were performed using the Quantum Espresso software package,³⁴ ultra-soft GBRV pseudopotentials,³⁵ a wave function cutoff of 40 Ry and a charge density cutoff of 200 Ry. The cluster was placed in a cubic box with linear dimensions of 45 Å and a Gaussian smearing of 0.001 Ry was employed. The relaxations were stopped when the forces were converged to within 10^{-3} eV/Å. To test the accuracy of these pseudopotential calculations, we also carried out all-electron relaxations using the FHIaims code.^{36,37} In these calculations, we also used the PBE exchange-correlation functional and second tier basis functions of numerical localized orbitals. Finally, for each cluster, the lowest-energy atomic structure was determined by comparing the total energies of all relaxed candidate structures in all possible spin states. For this, we used the local density approximation (LDA) and norm-conserving Hartwigsen-Goedecker-Hutter pseudopotentials³⁸ (including semicore states for the transition metal atoms) as implemented in the Octopus code^{39–42} (which was also used for the time-dependent DFT calculations of excited-state properties). In the Octopus code, the Kohn-Sham wavefunctions are calculated on a real-space grid. The grid spacing and box size were converged for each system, see Appendix.

For the lowest-energy relaxed structures, excited-state properties were obtained using time-dependent density-functional theory (TDDFT). Specifically, absorption spectra were calculated using a real-time propagation of the time-dependent Kohn-Sham orbitals following a delta-function perturbation. In these calculations, the time step is chosen sufficiently small to ensure a high degree of total energy conservation over the total propagation time of 13.164 fs. All convergence parameters used are listed in the Appendix.

To analyze light-induced charge transfer between cluster and CO₂ molecule, we also carry out linear-response TDDFT calculations. For this, we solve the Casida equation⁴³ which has the form of an eigenvalue problem. The eigenvalues ω_I have the interpretation of excited

state energies. Casida proposed that the eigenvectors $F_{I,cv}$ can be used to construct an approximate wavefunction of the excited state.⁴³ Specifically, $C_{I,cv} = \sqrt{(\epsilon_c - \epsilon_v)/\omega_I} F_{I,cv}$ denotes the coefficient of the singly excited Slater determinant $|\Psi_{cv}\rangle = a_c^\dagger a_v |\Psi_0\rangle$ in the excited state I , with ϵ_c and ϵ_v being the Kohn-Sham energies of unoccupied and occupied states, respectively. These quantities can be used to calculate the light-induced charge transfer (LICT) in the excited state I as

$$LICT_I = f_I(Q_0 - Q_I) = f_I \sum_{cv} (q_c - q_v) |C_{I,cv}|^2, \quad (1)$$

where Q_I and Q_0 denote the amount of charge localized on the CO_2 molecule in the excited state I and the ground state, respectively, and f_I is the oscillator strength. Also, q_c and q_v are the amount of charge localized on the molecule in the unoccupied conduction c and occupied valence v Kohn-Sham orbitals obtained by projecting the Kohn-Sham wavefunctions onto the atomic orbitals of the CO_2 molecule. Note that a positive value of the $LICT$ indicates that electrons are transferred from the cluster onto the CO_2 molecule. We note that $LICT$ is often analyzed using the transition densities of the excited state.^{44–46} We have compared the $LICT$ from our approach with the one obtained from transition densities for several excited states and found good qualitative agreement between the two approaches. To converge the optical spectra from the linear-response approach, 100 unoccupied states in each spin channel were included.

Results

Table 1 summarizes the results of the geometry relaxations of the transition-metal doped Al clusters with CO_2 molecules. In all clusters except $[\text{Al}_{12}\text{Zr}]$ the relaxed structures are distorted icosahedra. The distortion is caused by the transition-metal dopant (and not by the presence of the CO_2 molecule). The almost perfect icosahedral geometry of $[\text{Al}_{12}\text{Zr}]$ can be explained by its valence electron number which is 40 (not counting the 8 semi-core

electrons). This is equal to the number of electrons in $[\text{Al}_{13}]^-$ which is also referred to as a "magic" cluster due to its closed shell, perfect icosahedral geometry and comparably high stability.⁴⁷


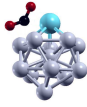

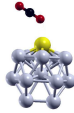
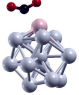
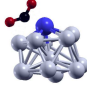
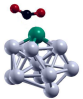
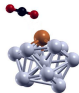
Adsorption distances, defined as the smallest distance between a cluster atom and an atom of the CO_2 , range from 1,8 Å to 2,4 Å for the doped clusters. In comparison, the adsorption distance between CO_2 and the un-doped neutral $[\text{Al}_{13}]$ cluster is significantly larger with 3,6 Å. The smallest adsorption distances are found for $[\text{Al}_{12}\text{Mn}]-\text{CO}_2$, $[\text{Al}_{12}\text{Co}]-\text{CO}_2$ and $[\text{Al}_{12}\text{Zr}]-\text{CO}_2$, while the biggest ones occur for $[\text{Al}_{12}\text{Fe}]-\text{CO}_2$ and $[\text{Al}_{12}\text{Cu}]-\text{CO}_2$. Except in $[\text{Al}_{12}\text{Zr}]-\text{CO}_2$ (where the CO_2 is closest to one of the Al atoms neighboring the Zr), the most favorable adsorption site is the transition metal dopant.

For all clusters except $[\text{Al}_{12}\text{Fe}]$ and $[\text{Al}_{12}\text{Cu}]$, the bond angle of the adsorbed CO_2 differs significantly from the value of the isolated molecule which is 180° . The deviation from linearity increases as the adsorption distance is reduced. For example, $[\text{Al}_{12}\text{Co}]-\text{CO}_2$ with an adsorption distance of 1,8 Å has a bond-angle of 135.5° , while $[\text{Al}_{12}\text{Ru}]-\text{CO}_2$ with an adsorption distance of 2,1 Å has a bond-angle of 142.9° . The bending of CO_2 reduces the energy of the lowest unoccupied energy levels and therefore facilitates transfer of electrons onto the CO_2 .⁵ This is often referred to as catalytic activation of the CO_2 molecule.

Table 2 summarizes the electronic ground state properties of the various clusters with and without CO_2 . As expected, systems with small adsorption distance have a large adsorption energy defined as the total energy difference of the relaxed system and its isolated ingredients (with each system being in its lowest-energy spin state). For example, $[\text{Al}_{12}\text{Zr}]-\text{CO}_2$ and $[\text{Al}_{12}\text{Co}]-\text{CO}_2$ (both with an adsorption distance of 1,8 Å) have an adsorption energy of -2.0 eV, while $[\text{Al}_{12}\text{Fe}]-\text{CO}_2$ and $[\text{Al}_{12}\text{Cu}]-\text{CO}_2$ both have adsorption energies of -0.3 eV.

In all systems except $[\text{Al}_{12}\text{Fe}]-\text{CO}_2$ and $[\text{Al}_{12}\text{Cu}]-\text{CO}_2$, adsorption is accompanied by a significant charge transfer between cluster and CO_2 . Using a Hirshfeld analysis,⁴⁸ we find that up to 0.36 electrons are transferred into the CO_2 . The largest charge transfer is found in $[\text{Al}_{12}\text{Zr}-\text{CO}_2]$ which has an adsorption distance of 1,9 Å and one of the highest adsorption

Table 1: Relaxed structures of $[\text{Al}_{13}]$ and $[\text{Al}_{12}M]$ clusters with adsorbed CO_2 . The adsorption distance is defined as the minimum distance between any molecular and any cluster atom (the relevant atoms are specified in brackets). The third column shows the O-C-O angle in degrees.

System	Adsorption distance [Å]	O-C-O angle [°]	System	Adsorption distance [Å]	O-C-O angle [°]
					
$[\text{Al}_{13}]-\text{CO}_2$	3.6 (C-Al)	177.7	$[\text{Al}_{12}\text{Zr}]-\text{CO}_2$	1.9 (O-Al)	131.4
					
$[\text{Al}_{12}\text{Mn}]-\text{CO}_2$	1.8 (C-Mn)	137.1	$[\text{Al}_{12}\text{Fe}]-\text{CO}_2$	2.4 (O-Fe)	179.7
					
$[\text{Al}_{12}\text{Ru}]-\text{CO}_2$	2.1 (C-Ru)	142.9	$[\text{Al}_{12}\text{Co}]-\text{CO}_2$	1.8 (C-Co)	135.5
					
$[\text{Al}_{12}\text{Ni}]-\text{CO}_2$	2.0 (O-Ni)	146.2	$[\text{Al}_{12}\text{Cu}]-\text{CO}_2$	2.3 (O-Cu)	179.3

energies of -2.0 eV. Interestingly, systems with small adsorption energies ($[\text{Al}_{12}\text{Fe}]-\text{CO}_2$ and $[\text{Al}_{12}\text{Cu}]-\text{CO}_2$) have a small charge transfer in the opposite directions, i.e. electrons are transferred from the CO_2 onto the cluster.

Further insight into the ground state electronic structure can be obtained from the electron localization function (ELF), see Figure 1. The ELF is a qualitative measure for the localization character of electrons.⁴⁹ In all systems which exhibit electron transfer onto the CO_2 molecule, an additional lobe in the ELF appears at the carbon atom with the lobe pointing towards the cluster. The value of the ELF in the lobe is close to unity indicating the presence of a highly localized electron. This is consistent with the expectation for a negatively charged CO_2 molecule where the presence of an additional electron results in a so-called "Umpolung" of the carbon dioxide molecule, i.e. the partial charge of the carbon changes sign compared to the neutral molecule.⁵ Comparing the ELF's of the transition metal doped clusters with adsorbed CO_2 to the undoped $[\text{Al}_{13}]-\text{CO}_2$, we find that the most important changes to the electronic structure are localized to the region near the dopant.

Table 2 also shows the spin states and the vertical and adiabatic ionization potentials (vertical IPs were calculated using the Delta-SCF method, adiabatic ones were obtained from the difference in total energies of the relaxed ionized system and that of the relaxed neutral system) of the cluster with CO_2 and compares them to the corresponding values of the isolated clusters without CO_2 . For the isolated clusters, we find that $[\text{Al}_{12}\text{Zr}]$, $[\text{Al}_{12}\text{Ru}]$ and $[\text{Al}_{12}\text{Ni}]$ have a singlet ground state and that $[\text{Al}_{12}\text{Cu}]$ has a doublet ground state. In contrast, high-spin ground states are obtained for $[\text{Al}_{12}\text{Mn}]$ (sextet), $[\text{Al}_{12}\text{Fe}]$ (quintet) and $[\text{Al}_{12}\text{Co}]$ (quartet). Upon addition of the CO_2 , only the spin state of the $[\text{Al}_{12}\text{Co}]$ and the $[\text{Al}_{12}\text{Mn}]$ system changes with $[\text{Al}_{12}\text{Co}-\text{CO}_2]$ and $[\text{Al}_{12}\text{Mn}-\text{CO}_2]$ both being a doublet. Both of these systems have a very small adsorption distance and exhibit a large electron transfer into the CO_2 .

The vertical ionization energies of the isolated clusters range from 6.2 eV (for $[\text{Al}_{12}\text{Zr}]$, $[\text{Al}_{12}\text{Mn}]$, $[\text{Al}_{12}\text{Fe}]$, $[\text{Al}_{12}\text{Ru}]$) to 6.5 eV in $[\text{Al}_{12}\text{Cu}]$. In all systems except for $[\text{Al}_{12}\text{Fe}]$ and

[Al₁₂Cu], addition of the CO₂ results in an increase of the ionization potential corresponding to an electronic stabilization of the system. This can be explained by the Nephelauxetic effect:⁵⁰ For systems with ground-state charge-transfer, the electron is localized over hybridized orbitals formed by the cluster and the molecule which reduces electron-electron repulsion. This also explains why the Mn and the Co doped clusters change their spin-multiplicity into a low-spin state upon CO₂ adsorption. The adiabatic ionization energies of the adsorbed systems are slightly smaller than their vertical counterparts for all systems except for [Al₁₂Ru]–CO₂ where it is the same. It is worth noting that relaxation after ionization leads to strong distortions in [Al₁₂Fe]–CO₂, [Al₁₂Mn]–CO₂ and [Al₁₂Ni]–CO₂, resulting in a more flattened geometry and in the case of the Ni doped cluster in an increase of adsorption distance and a change in CO₂ bond angle which results in a linear molecule. The spin multiplicity of the ionized systems is equal to the multiplicity of the neutral system -1 in all cases except for ([Al₁₂Mn]–CO₂)⁺. Instead of being a singlet, the resulting spin state is a triplet.

Comparison of the vertical with the adiabatic ionization potentials of the isolated clusters shows a decrease in ionization energy of 0.4 eV for the isolated Cu-doped cluster while all other clusters only exhibit minor changes. The main difference between the adiabatic ionization potentials and the vertical ones is the fact that from the adiabatic ionization potentials, the Cu-doped cluster unlike its Fe-doped counter-part does not get destabilized upon CO₂ adsorption but stabilized like the systems that show CO₂ activation. For the isolated clusters, the relaxed ionized clusters all have the spin multiplicity of the neutral isolated cluster -1 except for the Co doped cluster which results in a singlet spin state instead of the expected triplet.

Figure 2 shows the density of states (DOS) of all systems projected onto the CO₂ molecule. Two different scenarios are found: if the CO₂ molecule is weakly bound to the cluster (as in the case of [Al₁₂Cu]–CO₂ and [Al₁₂Fe]–CO₂), the projected DOS (pDOS) resembles that of the isolated molecule. In particular, the peak above the Fermi energy results from the lowest

Table 2: Electronic ground-state properties of $[Al_{12}M]$ clusters with adsorbed CO_2 , including the spin multiplicity, ionization energies, adsorption energy and the ground-state charge transfer (GS CT) into CO_2 (evaluated using Hirshfeld’s scheme⁴⁸). Values for the isolated clusters are given in brackets.

System	Spin multiplicity	Vertical ion- ization en- ergy [eV]	Adiabatic ionization energy [eV]	Adsorption Energy [eV]	GS into [e]	CT CO_2
$[Al_{12}Zr]-CO_2$	singlet (singlet)	6.3 (6.2)	6.1 (6.0)	-2.0	+0.36	
$[Al_{12}Mn]-CO_2$	doublet (sextet)	6.5 (6.2)	6.3 (6.0)	-1.5	+0.28	
$[Al_{12}Fe]-CO_2$	quintet (quintet)	6.0 (6.2)	5.8 (6.1)	-0.3	-0.08	
$[Al_{12}Ru]-CO_2$	singlet (singlet)	6.4 (6.2)	6.4 (6.2)	-1.2	+0.31	
$[Al_{12}Co]-CO_2$	doublet (quartet)	6.4 (6.3)	6.3 (6.2)	-2.0	+0.29	
$[Al_{12}Ni]-CO_2$	singlet (singlet)	6.7 (6.4)	6.5 (6.3)	-0.7	+0.20	
$[Al_{12}Cu]-CO_2$	doublet (doublet)	6.4 (6.5)	6.3 (6.1)	-0.3	-0.07	

unoccupied molecular orbital (LUMO) of the CO_2 while the peak at ~ -6 eV corresponds to the CO_2 HOMO. There are no peaks in the vicinity of the Fermi level. In contrast, the pDOS of systems with strong CO_2 adsorption (all systems except $[Al_{12}Cu]-CO_2$ and $[Al_{12}Fe]-CO_2$) exhibits a large number of peaks as a consequence of hybridization between molecular states and cluster states. Compared to the systems with weak adsorption, we find occupied states with partial CO_2 character relatively close to the Fermi level. These states contain the extra electrons that appear on CO_2 in the Hirshfeld analysis as a result of hybridisation between occupied cluster and unoccupied molecular orbitals, see Table 2.

Next, we consider excited states of the transition metal doped Al clusters with CO_2 molecules. Fig. 3 shows the absorption spectra of all systems with and without the CO_2 . All spectra have an onset between 3 and 4 eV and exhibit a peak between 5 and 6 eV with the detailed shape of the spectrum depending on the transition metal dopant and the cluster geometry. In $[Al_{12}Cu]-CO_2$ and $[Al_{12}Fe]-CO_2$, the presence of the CO_2 molecule does not modify the absorption spectrum significantly. This is not surprising as the CO_2 molecule has a large HOMO-LUMO gap ($\text{eigenenergy}(CO_2\text{LUMO}) - \text{eigenenergy}(CO_2\text{HOMO}) = 8.5$ eV according to our calculations and the findings of Kim et al.⁵²) and the interaction between cluster and molecule is weak. In the other systems, small differences can be observed,

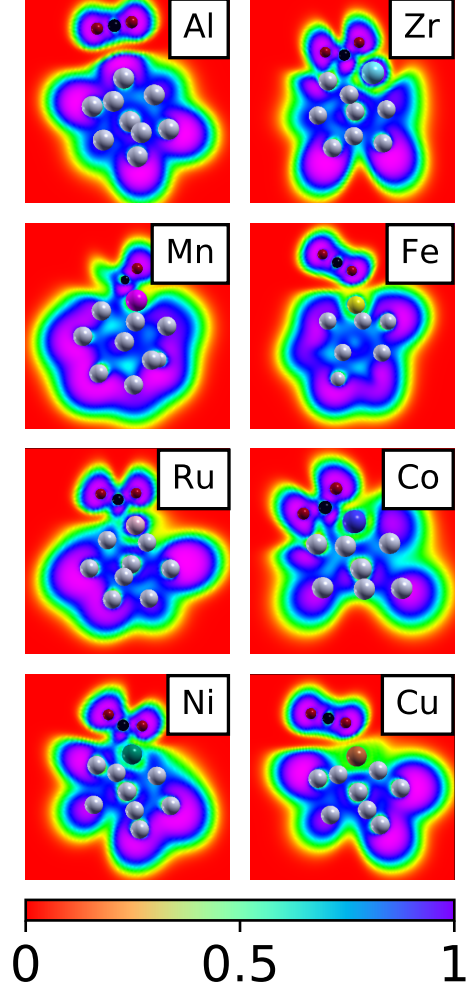


Figure 1: Electron localization function (ELF) of the transition-metal doped Al clusters with CO_2 . For comparison, the ELF of a neutral $[\text{Al}_{13}]$ cluster with CO_2 is also shown (upper left picture).

however. For example, the presence of the CO_2 results in a noticeable blue-shift of the main absorption peak near 5.5 eV in $[\text{Al}_{12}\text{Ni}]-\text{CO}_2$.

Finally, we investigate the light-induced charge transfer between the clusters and the CO_2 . Fig. 4 shows the amount of transferred charge as function of the excitation energy. First, we observe that $[\text{Al}_{12}\text{Cu}]$ and $[\text{Al}_{12}\text{Fe}]$ only transfer electrons into the CO_2 . This is expected as there is no charge transfer in the ground state for these systems and the CO_2 HOMO lies far below the Fermi level, see Fig. 2. As the CO_2 LUMO is closer to the Fermi level in the $[\text{Al}_{12}\text{Fe}]-\text{CO}_2$ system compared to the $[\text{Al}_{12}\text{Cu}]-\text{CO}_2$ system, the onset of LICT

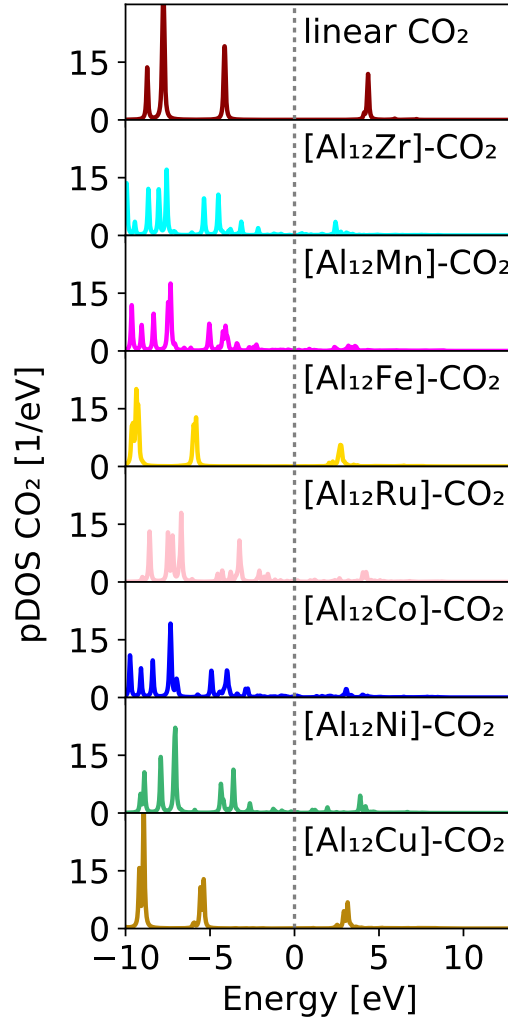


Figure 2: DOS projected onto CO_2 atomic orbitals for transition metal doped aluminium cluster with adsorbed CO_2 . The zero of energy is set to the Fermi level and denoted by a grey vertical line. A broadening of 0.05 eV has been used. For comparison, we also show the DOS of an isolated CO_2 molecule.

occurs at somewhat lower excitation energies. In contrast, $[\text{Al}_{12}\text{Ru}]-\text{CO}_2$ and $[\text{Al}_{12}\text{Mn}]-\text{CO}_2$ exhibit mostly LICT in the opposite direction, i.e. electrons are transferred from the CO_2 to the cluster. This can be interpreted as a back-transfer of those electrons that move onto the cluster in the ground state, see Table 2. Among these systems, the back-transfer is most pronounced in the Ru-doped cluster and already starts at low excitation energies of ~ 2 eV. Inspecting the pDOS of the Ru-cluster, Fig. 2, we see that this system exhibits hybridized occupied states close to the Fermi level. In the Mn-doped system, however, LICT

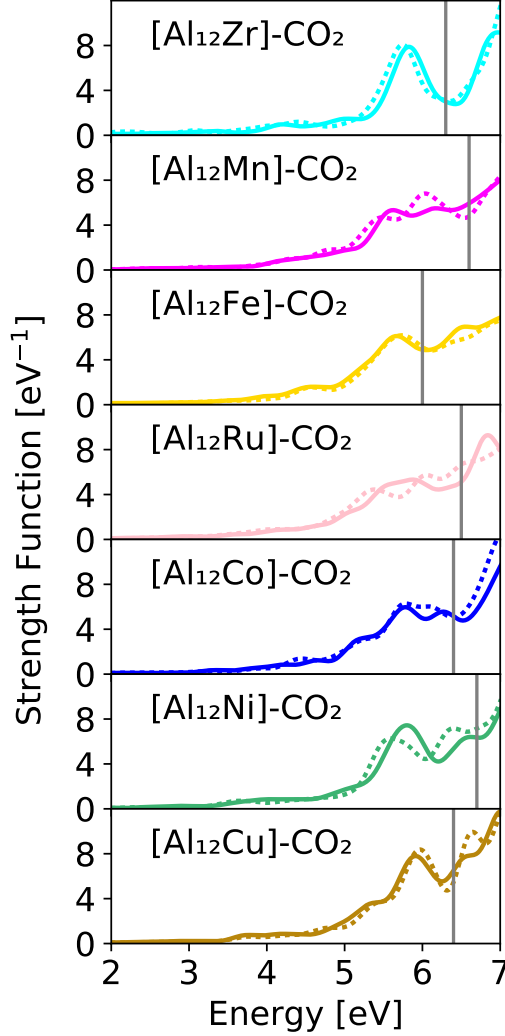


Figure 3: Absorption spectra of the transition metal doped Al clusters with (solid lines) and without (dashed lines) adsorbed CO_2 . The strength function is proportional to the absorption cross section.⁵¹ The vertical grey line denotes the first vertical ionization energy of each system.

is relatively small and only occurs at high excitation energies. This is caused by the fact that the Mn-doped cluster undergoes a transition from high-spin to a low-spin ground state when in contact with the CO_2 (see Table 2), making a back-transfer less favorable than in the Ru-doped system where the spin state is not affected by the presence of the CO_2 . A similar situation occurs for the Co-doped system. Finally, for $[\text{Al}_{12}\text{Zr}]-\text{CO}_2$, $[\text{Al}_{12}\text{Co}]-\text{CO}_2$ and $[\text{Al}_{12}\text{Ni}]-\text{CO}_2$, LICT can occur in both directions. Interestingly, $[\text{Al}_{12}\text{Zr}]-\text{CO}_2$ and $[\text{Al}_{12}\text{Co}]-\text{CO}_2$ exhibit only a small reduction of the ionization energy upon CO_2 adsorption.

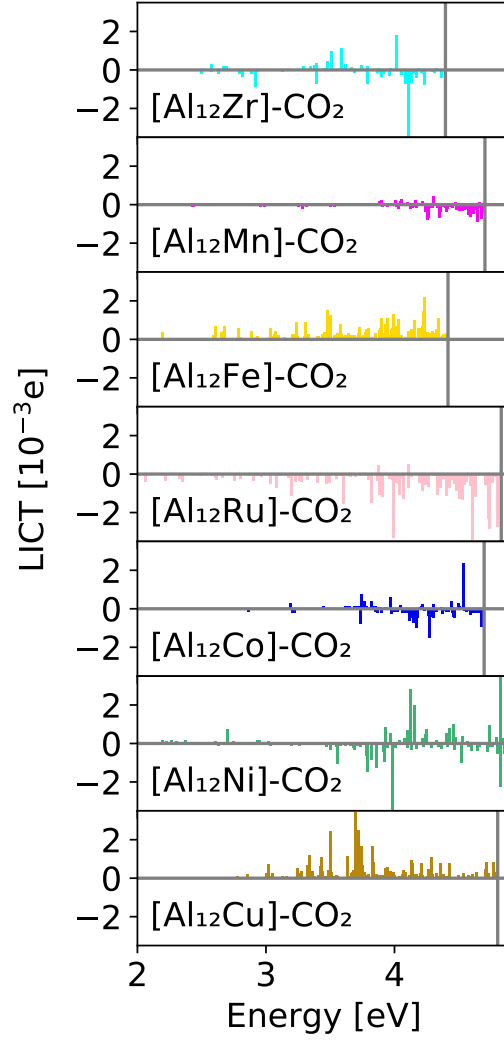


Figure 4: Light-induced charge transfer (LICT) in units of elementary charge e as function of excitation energy between transition metal doped Al clusters and CO_2 . Grey vertical lines indicate the threshold energy above which the excited states contain a significant fraction (more than five percent) of Kohn-Sham orbitals above the vacuum level.

This suggests that the transferred electrons in these systems originate from delocalized cluster orbitals such that additional electron transfer in the excited state does not result in a large energy cost due to repulsive electron-electron interactions.

Discussion and conclusions

We have studied the atomic and electronic properties of transition metal doped aluminium clusters with adsorbed CO_2 using first-principles density-functional theory and also time-dependent density-functional theory. Our results suggest that the set of transition-metal doped aluminium clusters can be divided into two categories: (i) clusters which strongly adsorb CO_2 with significant ground state charge transfer and (ii) clusters with weak CO_2 adsorption and no significant ground state charge transfer. The clusters in class (ii) are $[\text{Al}_{12}\text{Cu}]$ and $[\text{Al}_{12}\text{Fe}]$, while all other systems ($[\text{Al}_{12}\text{Zr}]$, $[\text{Al}_{12}\text{Mn}]$, $[\text{Al}_{12}\text{Ru}]$, $[\text{Al}_{12}\text{Co}]$, $[\text{Al}_{12}\text{Ni}]$) belong to class (i). Systems in class (ii) exhibit light-induced electron transfer into the CO_2 . In contrast, light-induced electron back-transfer from the CO_2 to the cluster dominates in class (i) systems, but light-induced electron transfer is also possible when the CO_2 adsorption does not result in significant changes to the ionization energy (as in the cases of $[\text{Al}_{12}\text{Zr}]$ and $[\text{Al}_{12}\text{Co}]$). In conclusion, our work contributes to a detailed understanding of the effect of transition metal doping on ground- and excited-state charge transfer and paves the way towards a rational design of atomically defined photo-catalysts for CO_2 conversion.

Acknowledgement

This work was supported by the European Research Council (ERC-2015-AdG694097), the Cluster of Excellence ‘Advanced Imaging of Matter’ (AIM), Grupos Consolidados (IT1249-19), SFB925 ”Light induced dynamics and control of correlated quantum systems” and by the Deutsche Forschungsgemeinschaft (DFG) through the Research Training Group -Quantum Mechanical Materials Modelling - GRK 2247. The Flatiron Institute is a division of the Simons Foundation.

References

- (1) Chang, X.; Wang, T.; Gong, J. CO₂ photo-reduction: insights into CO₂ activation and reaction on surfaces of photocatalysts. *Energy & Environmental Science* **2016**, *9*, 2177–2196.
- (2) Remiro-Buenamañana, S.; García, H. Photoassisted CO₂ conversion to fuels. *ChemCatChem* **2019**, *11*, 342–356.
- (3) Rodemerck, U.; Holeňa, M.; Wagner, E.; Smejkal, Q.; Barkschat, A.; Baerns, M. Catalyst development for CO₂ hydrogenation to fuels. *ChemCatChem* **2013**, *5*, 1948–1955.
- (4) Kumar, B.; Llorente, M.; Froehlich, J.; Dang, T.; Sathrum, A.; Kubiak, C. P. Photochemical and photoelectrochemical reduction of CO₂. *Annual review of physical chemistry* **2012**, *63*, 541–569.
- (5) Álvarez, A.; Borges, M.; Corral-Pérez, J. J.; Olcina, J. G.; Hu, L.; Cornu, D.; Huang, R.; Stoian, D.; Urakawa, A. CO₂ activation over catalytic surfaces. *ChemPhysChem* **2017**, *18*, 3135–3141.
- (6) Kho, E. T.; Tan, T. H.; Lovell, E.; Wong, R. J.; Scott, J.; Amal, R. A review on photo-thermal catalytic conversion of carbon dioxide. *Green Energy & Environment* **2017**, *2*, 204–217.
- (7) Hussin, F.; Aroua, M. K. Recent development in the electrochemical conversion of carbon dioxide: Short review. AIP Conference Proceedings. 2019; p 030017.
- (8) Puliyalil, H.; Jurković, D. L.; Dasireddy, V. D.; Likožar, B. A review of plasma-assisted catalytic conversion of gaseous carbon dioxide and methane into value-added platform chemicals and fuels. *RSC advances* **2018**, *8*, 27481–27508.
- (9) Graf, E.; Leitner, W. Direct formation of formic acid from carbon dioxide and dihydro-

- gen using the $[\{\text{Rh}(\text{cod})\text{Cl}\}_2]\text{-Ph}_2\text{P}(\text{CH}_2)_4\text{PPh}_2$ catalyst system. *Journal of the Chemical Society, Chemical Communications* **1992**, 623–624.
- (10) Costentin, C.; Passard, G.; Robert, M.; Savéant, J.-M. Ultraefficient homogeneous catalyst for the CO₂-to-CO electrochemical conversion. *Proceedings of the National Academy of Sciences* **2014**, *111*, 14990–14994.
 - (11) Filonenko, G. A.; Hensen, E. J.; Pidko, E. A. Mechanism of CO₂ hydrogenation to formates by homogeneous Ru-PNP pincer catalyst: from a theoretical description to performance optimization. *Catalysis Science & Technology* **2014**, *4*, 3474–3485.
 - (12) Wang, W.; Wang, S.; Ma, X.; Gong, J. Recent advances in catalytic hydrogenation of carbon dioxide. *Chemical Society Reviews* **2011**, *40*, 3703–3727.
 - (13) Prasad, P. S.; Bae, J. W.; Jun, K.-W.; Lee, K.-W. Fischer–Tropsch synthesis by carbon dioxide hydrogenation on Fe-based catalysts. *Catalysis surveys from Asia* **2008**, *12*, 170–183.
 - (14) Nakamura, J.; Choi, Y.; Fujitani, T. On the issue of the active site and the role of ZnO in Cu/ZnO methanol synthesis catalysts. *Topics in catalysis* **2003**, *22*, 277–285.
 - (15) Chang, F.-W.; Hsiao, T.-J.; Shih, J.-D. Hydrogenation of CO₂ over a rice husk ash supported nickel catalyst prepared by deposition-precipitation. *Industrial & engineering chemistry research* **1998**, *37*, 3838–3845.
 - (16) Li, G.; Jin, R. Atomically precise gold nanoclusters as new model catalysts. *Accounts of chemical research* **2013**, *46*, 1749–1758.
 - (17) Tang, Q.; Lee, Y.; Li, D.-Y.; Choi, W.; Liu, C.; Lee, D.; Jiang, D.-e. Lattice-hydride mechanism in electrocatalytic CO₂ reduction by structurally precise copper-hydride nanoclusters. *Journal of the American Chemical Society* **2017**, *139*, 9728–9736.

- (18) Jin, R.; Li, G.; Sharma, S.; Li, Y.; Du, X. Toward Active-Site Tailoring in Heterogeneous Catalysis by Atomically Precise Metal Nanoclusters with Crystallographic Structures. *Chemical Reviews* **2020**,
- (19) Zhu, Y.; Qian, H.; Jin, R. Catalysis opportunities of atomically precise gold nanoclusters. *Journal of Materials Chemistry* **2011**, *21*, 6793–6799.
- (20) Kauffman, D. R.; Alfonso, D.; Matranga, C.; Ohodnicki, P.; Deng, X.; Siva, R. C.; Zeng, C.; Jin, R. Probing active site chemistry with differently charged Au₂₅ q nanoclusters (q = -1, 0, +1). *Chemical Science* **2014**, *5*, 3151–3157.
- (21) Fei, W.; Antonello, S.; Dainese, T.; Dolmella, A.; Lahtinen, M.; Rissanen, K.; Venzo, A.; Maran, F. Metal Doping of Au₂₅ (SR)₁₈-Clusters: Insights and Hints. *Journal of the American Chemical Society* **2019**, *141*, 16033–16045.
- (22) Knight, M. W.; King, N. S.; Liu, L.; Everitt, H. O.; Nordlander, P.; Halas, N. J. Aluminum for plasmonics. *ACS nano* **2014**, *8*, 834–840.
- (23) Gérard, D.; Gray, S. K. Aluminium plasmonics. *Journal of Physics D: Applied Physics* **2014**, *48*, 184001.
- (24) Martin, J.; Plain, J. Fabrication of aluminium nanostructures for plasmonics. *Journal of Physics D: Applied Physics* **2014**, *48*, 184002.
- (25) Moscatelli, A. Plasmonics: the aluminium rush. *Nature nanotechnology* **2012**, *7*, 778.
- (26) Clavero, C. Plasmon-induced hot-electron generation at nanoparticle/metal-oxide interfaces for photovoltaic and photocatalytic devices. *Nature Photonics* **2014**, *8*, 95–103.
- (27) González, J.; Lopez, V.; Bautista, A.; Otero, E.; Nóvoa, X. Characterization of porous aluminium oxide films from ac impedance measurements. *Journal of applied Electrochemistry* **1999**, *29*, 229–238.

- (28) Robatjazi, H.; Zhao, H.; Swearer, D. F.; Hogan, N. J.; Zhou, L.; Alabastri, A.; McClain, M. J.; Nordlander, P.; Halas, N. J. Plasmon-induced selective carbon dioxide conversion on earth-abundant aluminum-cuprous oxide antenna-reactor nanoparticles. *Nature communications* **2017**, *8*, 1–10.
- (29) Swearer, D. F.; Leary, R. K.; Newell, R.; Yazdi, S.; Robatjazi, H.; Zhang, Y.; Renard, D.; Nordlander, P.; Midgley, P. A.; J, H. N. Transition-metal decorated aluminum nanocrystals. *ACS nano* **2017**, *11*, 10281–10288.
- (30) Zhao, J.-Y.; Zhang, Y.; Zhao, F.-Q.; Ju, X.-H. Adsorption of Carbon Dioxide on Al₁₂X Clusters Studied by Density Functional Theory: Effect of Charge and Doping. *The Journal of Physical Chemistry A* **2013**, *117*, 12519–12528.
- (31) Zhao, J.-Y.; Zhao, F.-Q.; Xu, S.-Y.; Ju, X.-H. Theoretical study of the geometries and decomposition energies of CO₂ on Al₁₂X: Doping effect of Al₁₂X. *Journal of Molecular Graphics and Modelling* **2014**, *48*, 9–17.
- (32) Perdew, J. P.; Burke, K.; Ernzerhof, M. Generalized gradient approximation made simple. *Physical review letters* **1996**, *77*, 3865.
- (33) Grimme, S.; Antony, J.; Ehrlich, S.; Krieg, H. A consistent and accurate ab initio parametrization of density functional dispersion correction (DFT-D) for the 94 elements H-Pu. *The Journal of chemical physics* **2010**, *132*, 154104.
- (34) Giannozzi, P.; Baroni, S.; Bonini, N.; Calandra, M.; Car, R.; Cavazzoni, C.; Ceresoli, D.; Chiarotti, G. L.; Cococcioni, M.; Dabo, I. QUANTUM ESPRESSO: a modular and open-source software project for quantum simulations of materials. *Journal of physics: Condensed matter* **2009**, *21*, 395502.
- (35) Garrity, K. F.; Bennett, J. W.; Rabe, K. M.; Vanderbilt, D. Pseudopotentials for high-throughput DFT calculations. *Computational Materials Science* **2014**, *81*, 446–452.

- (36) Blum, V.; Gehrke, R.; Hanke, F.; Havu, P.; Havu, V.; Ren, X.; Reuter, K.; Scheffler, M. Ab initio molecular simulations with numeric atom-centered orbitals. *Computer Physics Communications* **2009**, *180*, 2175–2196.
- (37) Havu, V.; Blum, V.; Havu, P.; Scheffler, M. Efficient O (N) integration for all-electron electronic structure calculation using numeric basis functions. *Journal of Computational Physics* **2009**, *228*, 8367–8379.
- (38) Hartwigsen, C.; Goedecker, S.; Hutter, J. Relativistic separable dual-space Gaussian pseudopotentials from H to Rn. *Physical Review B* **1998**, *58*, 3641.
- (39) Castro, A.; Appel, H.; Oliveira, M.; Rozzi, C. A.; Andrade, X.; Lorenzen, F.; Marques, M. A.; Gross, E.; Rubio, A. Octopus: a tool for the application of time-dependent density functional theory. *physica status solidi (b)* **2006**, *243*, 2465–2488.
- (40) Andrade, X.; Strubbe, D.; De Giovannini, U.; Larsen, A. H.; Oliveira, M. J.; Alberdi-Rodriguez, J.; Varas, A.; Theophilou, I.; Helbig, N.; Verstraete, M. J. Real-space grids and the Octopus code as tools for the development of new simulation approaches for electronic systems. *Physical Chemistry Chemical Physics* **2015**, *17*, 31371–31396.
- (41) Tancogne-Dejean, N.; Oliveira, M. J.; Andrade, X.; Appel, H.; Borca, C. H.; Le Breton, G.; Buchholz, F.; Castro, A.; Corni, S.; Correa, A. A. Octopus, a computational framework for exploring light-driven phenomena and quantum dynamics in extended and finite systems. *The Journal of Chemical Physics* **2020**, *152*, 124119.
- (42) Tancogne-Dejean, N.; Oliveira, M. J.; Rubio, A. Self-consistent DFT+ U method for real-space time-dependent density functional theory calculations. *Physical Review B* **2017**, *96*, 245133.
- (43) Casida, M. E. *Recent Advances In Density Functional Methods: (Part I)*; World Scientific, 1995; pp 155–192.

- (44) Zong, H.; Wang, X.; Quan, J.; Tian, C.; Sun, M. Photoinduced charge transfer by one and two-photon absorptions: physical mechanisms and applications. *Physical Chemistry Chemical Physics* **2018**, *20*, 19720–19743.
- (45) Plasser, F.; Lischka, H. Analysis of excitonic and charge transfer interactions from quantum chemical calculations. *Journal of chemical theory and computation* **2012**, *8*, 2777–2789.
- (46) Sun, M.; Chen, J.; Xu, H. Visualizations of transition dipoles, charge transfer, and electron-hole coherence on electronic state transitions between excited states for two-photon absorption. *The Journal of chemical physics* **2008**, *128*, 064106.
- (47) Smith, Q. A.; Gordon, M. S. Electron affinity of Al₁₃: a correlated electronic structure study. *The Journal of Physical Chemistry A* **2011**, *115*, 899–903.
- (48) Hirshfeld, F. L. Bonded-atom fragments for describing molecular charge densities. *Theoretica chimica acta* **1977**, *44*, 129.
- (49) Becke, A. D.; Edgecombe, K. E. A simple measure of electron localization in atomic and molecular systems. *The Journal of chemical physics* **1990**, *92*, 5397–5403.
- (50) König, E. *The nephelauxetic effect calculation and accuracy of the interelectronic repulsion parameters (I. Cubic high-spin d 2, d 3, d 7, and d 8 systems) in "Structure and Bonding"*; Springer, 1971; pp 175–212.
- (51) Marques, M. A.; Castro, A.; Bertsch, G. F.; Rubio, A. octopus: a first-principles tool for excited electron–ion dynamics. *Computer Physics Communications* **2003**, *151*, 60–78.
- (52) Kim, C.; Hyeon, S.; Lee, J.; Kim, W. D.; Lee, D. C.; Kim, J.; Lee, H. Energy-efficient CO₂ hydrogenation with fast response using photoexcitation of CO₂ adsorbed on metal catalysts. *Nature communications* **2018**, *9*, 1–8.

Supporting Information Available

Table 3 and 4 summarize the convergence parameters that were used in this work.

Table 3: Calculation parameters used for determining the vertical ionization energy ("IP"), adsorption energy, adiabatic ionization energy and most favorable spin-state ("AE") and computation of DOS, pDOS, ELF's, ground-state electron transfer and Casida calculations ("DOS"). "Grid" denotes the spacing of points on the real-space grid while "Box" denotes the radius of the minimum box. In the calculation of the ELF of $[\text{Al}_{13}]-\text{CO}_2$, a smearing of 0.1 eV was used to achieve convergence.

System	Grid (IP) [Å]	Box (IP)[Å]	Grid (AE) [Å]	Box (AE) [Å]	Grid (DOS) [Å]	Box (DOS) [Å]
$[\text{Al}_{12}\text{Zr}]-\text{CO}_2$	0.18	5	0.06	5	0.16	9
$[\text{Al}_{12}\text{Mn}]-\text{CO}_2$	0.14	6	0.06	5	0.14	9
$[\text{Al}_{12}\text{Fe}]-\text{CO}_2$	0.18	5	0.06	5	0.16	9
$[\text{Al}_{12}\text{Ru}]-\text{CO}_2$	0.20	6	0.06	5	0.18	9
$[\text{Al}_{12}\text{Co}]-\text{CO}_2$	0.16	5	0.06	5	0.14	9
$[\text{Al}_{12}\text{Ni}]-\text{CO}_2$	0.12	5	0.06	5	0.14	9
$[\text{Al}_{12}\text{Cu}]-\text{CO}_2$	0.16	5	0.06	5	0.14	9

Table 4: Minimal convergence Parameters found for computation of the absorption spectra from time-propagations.

System	Time [1/eV]	Step	Grid [Å]	Box [Å]	Radius	kick strength [1/Å]
$[\text{Al}_{12}\text{Zr}]-\text{CO}_2$	0.001		0.26	8.0		0.01
$[\text{Al}_{12}\text{Mn}]-\text{CO}_2$	0.001		0.18	8.0		0.01
$[\text{Al}_{12}\text{Fe}]-\text{CO}_2$	0.001		0.22	8.0		0.01
$[\text{Al}_{12}\text{Ru}]-\text{CO}_2$	0.001		0.32	8.0		0.01
$[\text{Al}_{12}\text{Co}]-\text{CO}_2$	0.001		0.20	9.0		0.01
$[\text{Al}_{12}\text{Ni}]-\text{CO}_2$	0.001		0.18	8.0		0.01
$[\text{Al}_{12}\text{Cu}]-\text{CO}_2$	0.001		0.18	13.0		0.01

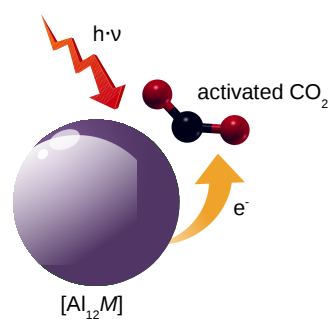


Figure 5: For Table of Contents Only.